RAA 2019 Vol. **19** No. **9**, 136(10pp) doi: 10.1088/1674–4527/19/9/136

http://www.raa-journal.org *http://iopscience.iop.org/raa*

Research in Astronomy and Astrophysics

Triple Range Imager and POLarimeter (TRIPOL) — a compact and economical optical imaging polarimeter for small telescopes

Shuji Sato[1], Po Chieh Huang[2], Wen Ping Chen[2], Takahiro Zenno[1], Chakali Eswaraiah[2*], Bo He Su[2], Shinsuke Abe[2**], Daisuke Kinoshita[2] and Jia Wei Wang[3]

[1] Astrophysics Department, Nagoya University, Nagoya, 464–8602, Japan

[2] Graduate Institute of Astronomy, NCU, Taoyuan 32001; *wchen@astro.ncu.edu.tw*

[3] Department of Physics and Institute of Astronomy, NTHU, Hsinchu 30013

Received 2019 March 13; accepted 2019 April 23

Abstract We report the design concept and performance of a compact, lightweight and economical imaging polarimeter, the Triple Range Imager and POLarimeter (TRIPOL), capable of simultaneous optical imagery and polarimetry. TRIPOL splits the beam in wavelengths from 400 to 830 nm into g'-, r'- and i'-bands with two dichroic mirrors, and measures polarization with an achromatic half-waveplate and a wire grid polarizer. The simultaneity makes TRIPOL a useful tool for small telescopes for the photometry and polarimetry of time variable and wavelength dependent phenomena. TRIPOL is designed for a Cassegrain telescope with an aperture of ∼1 m. This paper presents the engineering considerations of TRIPOL and compares the expected with observed performance. Using the Lulin 1-m telescope and 100 seconds of integration, the limiting magnitudes are $g' \sim 19.0$ mag, $r' \sim 18.5$ mag and $i' \sim 18.0$ mag with a signal-to-noise ratio of 10, in agreement with design expectation. The instrumental polarization is measured to be $\sim 0.3\%$ in the three bands. Two applications, one to the star-forming cloud IC 5146 and the other to the young variable GM Cep, are presented as demonstrations.

Key words: instrumentation: photometers — instrumentation: polarimeters — techniques: photometric — techniques: polarimetric — methods: observational — ISM: magnetic fields

1 INTRODUCTION

Polarization provides information about a celestial object in addition to that acquired by photometry and spectroscopy (Tinbergen 1996; Clarke 2010). Yet a polarimeter is considered to be a specialized instrument when fitted to an optical telescope with a small size aperture. Nowadays, with commercial CCD cameras and other optical and electronic components readily available with good performance, it has become feasible to design and fabricate a compact and economical polarimetric imager to be used for scientific programs with small telescopes. We report on an imaging system, Triple Range Imaging POLarimeter (TRIPOL), capable of simultaneous imaging photometry and polarimetry in three optical bands (g', r', i'). TRIPOL was designed for a telescope with a primary mirror of around one meter in diameter and located at a moderate observing site, with typical seeing of 1 to 2 arcsec. The telescope is assumed to have a Cassegrain f-ratio from F/6 to F/15, and the CCD pixel scale is from 10 to 20 µm to properly sample the point spread function. The optics uses no lenses to magnify or reduce the image, and the elements, such as dichroic mirrors, spectral filters, half-waveplate (HWP) and wire grid polarizer (WGP), are all flat and thin for easy optical alignment. TRIPOL is compact, measuring $300 \times 350 \times 250$ mm in width, length and height respectively, weighs only 15 kg including the data acquisition system, and is easy to operate. It was designed to an accuracy of $\sim 3''$ for alignment, and ~ 0.05 mm for machining and positioning. This paper describes the performance of the first (TRIPOL1) and second (TRIPOL2) units of

* Now at National Astronomical Observatories, Chinese Academy of Sciences, Beijing, China

** Now at Department of Aerospace Engineering, Nihon University, Japan

TRIPOL adapted for use on the Lulin One-meter Telescope (LOT) in Taiwan. In the F/8 beam of the LOT, and hence a $\sim$ $3°$ cone-angle, effects such as spherical aberration, chromatic aberration, and astigmatism are small compared to the 20 µm pixel size. We compare the design parameters with observational results on the polarization measurements of polarization standard stars, and demonstrate the use of TRIPOL when targeting the star-forming cloud IC 5146 and the young star GM Cep.

2 DESIGN OF TRIPOL

TRIPOL is composed of three parts, the polarization unit, the color-decomposition unit and the data-acquisition unit, plus three CCD cameras and a desktop computer. The overview and layout of the optical components are depicted in Figure 1. Light from the telescope passes through an HWP and a WGP, and is then decomposed by two dichroic mirrors (DM1 and DM2) and band-pass filters (BPFs) into three channels (g', r', i'). The incident photons are detected and converted to electrons in the CCD camera with built-in readout electronics.

The polarization unit, consisting of a rotatable HWP and a fixed WGP, working as a phase retarder and polarization analyzer, respectively, is located in front of the color-decomposition unit. The HWP, with size of 33 mm×33 mm and thickness of 3 mm, made of $\mathrm{SiO_2MgF_2}$, was procured from the optical shop Kogaku Giken Co. We employ a commercial (from Edmund Optics Co.) WGP plate composed of an Al wire grid, with size of 50 mm×50 mm and thickness of 1.5 mm, sandwiched by thin glass plates, affording a field-of-view as wide as the detector size. While using birefringent materials, such as a Wollaston prism, would allow for, alternatively, a dual beam design, thus minimizing instrumental and sky effects on polarization measurements, our design is much more compact and economical. The WGP is slightly tilted to avoid ghost images due to reflected glare.

For the color-decomposition unit, the central wavelengths (λ_0) and bandwidths ($\Delta\lambda$) are defined by multiplying the transmission or reflection curves of the DMs and BPFs for each of the g'-, r'- and i'-bands. The spectral response functions of the DMs and BPFs are shown in Figure 2.

Even though the TRIPOL optics makes no use of mirrors or lenses with power, astigmatism from tilted DMs and spherical aberration from flat-parallel BPFs may still exist. The g'-band optical train contains the BPF-g' and a CCD camera, the r'-band optical train holds DM1 tilted at an angle of $30°$, and the r'-i' optical train houses DM1 and DM2 at angles of $\pm 30°$.

Ray-tracing was executed using the software ZEMAX for classical Cassegrain-type telescopes with apertures D=0.7, 1.0 and 1.5 m, and f-ratios F/6, F/8, F/10, F/12.5 and F/15. We evaluated the tolerance of aberrations by comparing the root mean square (RMS) radius in the spot diagram with the detector pixel size and seeing size. It was confirmed that the RMS radius of the spot, due mostly to astigmatism, was smaller than 50 µm, or ∼2.5 times the pixel size, even near the corners of the detector, and much smaller than the seeing size, $1.5''$. With various parameters for apertures and focal ratios, the optics is found tolerable for an F/7 or slower beam. Astigmatism can be remedied by wedging DM1 and DM2 by $0.18°$ and $0.24°$, respectively, even for a system as fast as F/7.

TRIPOL was designed to use commercially available CCD cameras, with the specific model in accordance with scientific and budgetary requirements. TRIPOL1 and TRIPOL2 employed SBIG ST-9 XEi cameras using KAF-0261E plus TC-237, having 512×512 pixels, each with 20 µm on a side. The detector response shows linearity up to ∼50 000 counts, or about 1/3 of the full well. The dark current is 10 [e/s] at temperature $\sim$ 0°C and the readout noise is 15 [e] per sampling.

The CCD cameras are located on the bottom plate so as to align each of the array centers to the focal point of the telescope within an accuracy of less than 0.1 mm (∼5 pixels) relative to each other. The SBIG ST-9 camera model satisfied our initial need for point-source targets, but that model is no longer available. Subsequent TRIPOL units were upgraded to the camera model STT-8300. A computer (Intel DN2800MT) controls simultaneous readout of the three CCD cameras and the polarization units according to the position angles of the HWP via three USB 2.0 cables. The overall cost of TRIPOL, excluding the cameras and the computer, was about US$17 000 in 2010.

3 EVALUATION OF PERFORMANCE

In this section, we evaluate the performance of TRIPOL in photometric and polarimetric measurements. In each case, the engineering design parameters are compared with those measured in actual observations.

3.1 Limiting Magnitudes for Photometry

The limiting magnitudes of TRIPOL2 were measured in December 2012 using the LOT, for which each SBIG ST9-

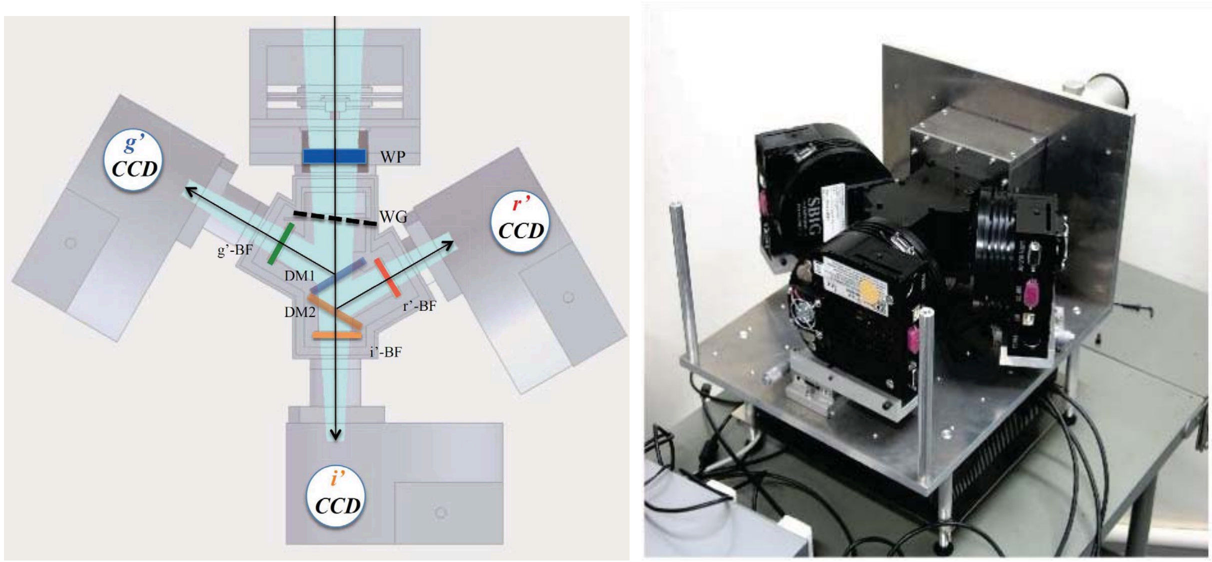

Fig. 1 (*Left*) Layout of the optical components and CCDs of TRIPOL2. *Arrows* illustrate the light paths. See the text for abbreviations. (*Right*) Overview of the components with the control computer utilized for data acquisition beneath the bottom plate.

XEi 20 μm pixel corresponds to $0.5''$, giving a field of view about $4.7' \times 4.7'$.

We observed the Landolt Field 101–404 (Landolt 1992) for 100 s, and analyzed the images of the 12 stars with a photometric aperture of $4.0''$, or 8 pixels in diameter, and derived the limiting magnitudes of 19, 18.5 and 18, for signal to noise ratio (S/N) $\sim$ 10, respectively, in the g'-, r'- and i'-bands. In every band, the measured and expected values are in agreement with each other within uncertainties of ~ 0.5 mag. For a photometry-only observing run, the WGP could be removed to gain an increase of about 60% in incident flux.

3.2 Efficiency and Reliability of Polarization Measurements

The combination of a rotatable HWP and a fixed WGP, as described in Section 2, follows the same design as the near-infrared (J, H, Ks) polarimeter, SIRPOL, on the InfraRed Survey Facility (Kandori et al. 2006, IRSF). Below, we describe the performance parameters measured in the laboratory, in comparison with observations of standard stars.

3.2.1 Efficiency of the polarization devices

The phase retarder of the HWP was designed and measured by Kogaku Giken Co. to be $180° \pm 2°$ over the wavelength range 400 to 950 nm (see Fig. 3(a)). The transmittance of the WGP was measured in this wavelength range in steps of $\Delta\lambda = 50$ nm. Two identical WGPs were arranged such that one was fixed while the other was rotatable. When rotating relative to each other, a silicone photodiode was illuminated with a white light through the intermediate BPFs of $\Delta\lambda = 50$ nm. A single rotation gives a double sinusoidal curve. Fitting with a sinusoidal curve, we obtain $I(\theta) = A \sin 2(\theta - \phi) + B$, where A is the amplitude, B the residual and ϕ the phase-difference. For this we parameterized the transmittances, $T_{\rm max}$ and $T_{\rm min}$, parallel and perpendicular to each other, as plotted in Figure 3(b) and Figure 3(c) respectively. The contrast parameter, defined as the extinction ratio, $T_{\rm max}/T_{\rm min}$, should be as high as possible (infinite for a perfect polarizer), but in practice is considered satisfactory with a value above ~ 100 to substantially suppress the perpendicular component of polarization, i.e., the crosstalk. The contrast parameter measured for TRIPOL, presented as Figure 3(d), increases toward long wavelengths and remains sufficiently high above 500 nm.

3.2.2 Observations of polarization standard stars

The TRIPOL images were reduced by standard procedures for bias and dark subtraction, and corrected with flat-fielding. For each polarization measurement, target frames acquired with each filter at four HWP positions were aligned using DAOPHOT (find, daomaster and daogrow) and IRAF (geomap and geotran) packages. Then multiple frames for each HWP were average-combined using IRAF/imcombine. These four images, taken at each of the four HWP positions, became the science images used for photometry and polarimetry.

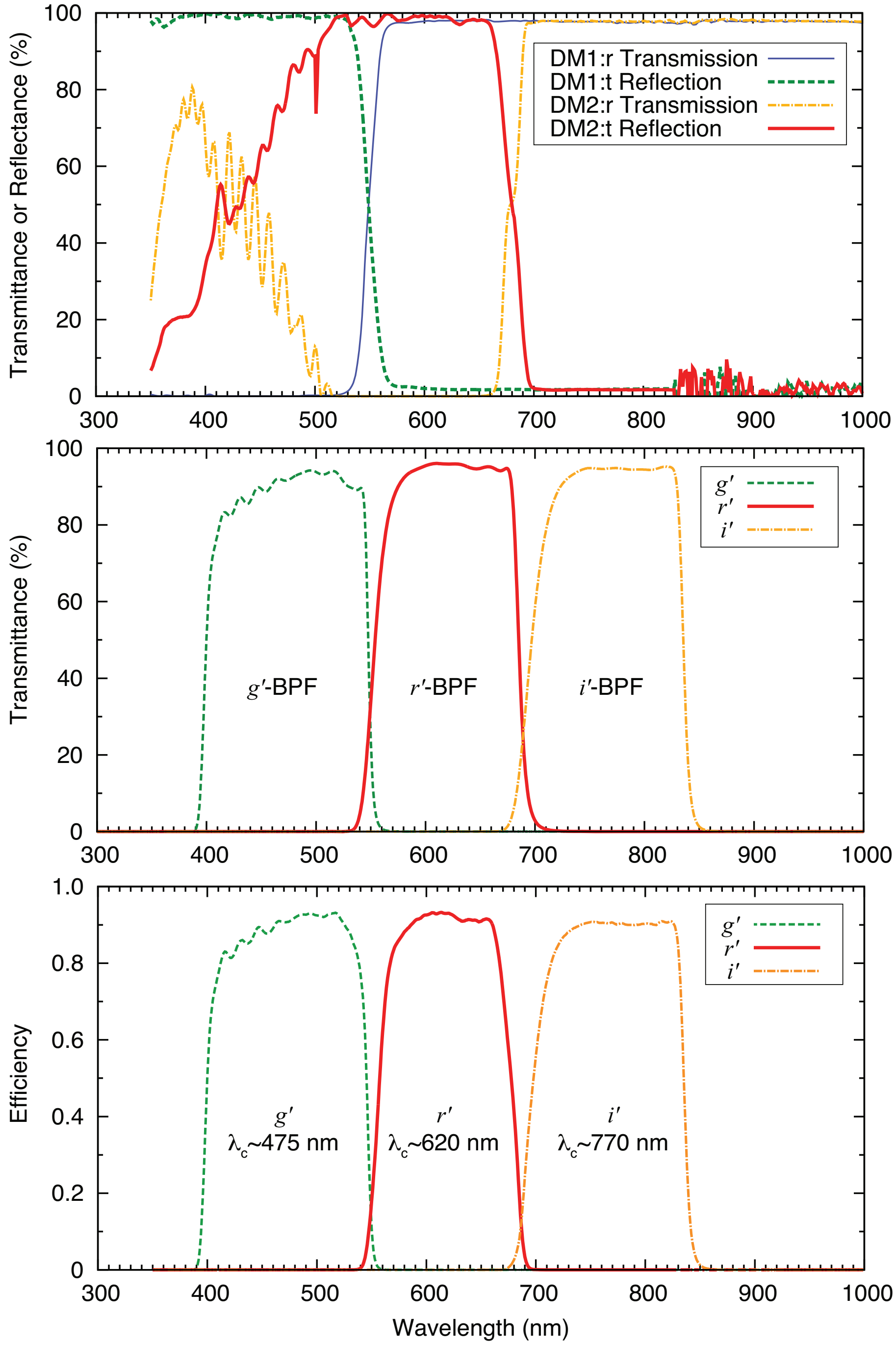

Fig. 2 Transmittance of optical components for the three passbands: (*top panel*) transmission/reflectance of the dichroic mirrors, (*middle panel*) transmission of the BPFs and (*bottom panel*) throughput.

Aperture photometry was performed using DAOFIND (for source detection with a threshold of 5σ for the sky variation) and PHOT (for aperture photometry) tasks of DAOPHOT for point sources. Typical image full widths at half maximum (FWHMs) for these runs varied between 2 and 4 pixels ($1'' - 2''$). The flux of a star at each position of the HWP was estimated using IRAF/DAOPHOT with an aperture size of 2.5 times the FWHM. The inner and outer sky annuli were chosen to be 5 and 10 pixels more than the star aperture. Fluxes at four angles are used to compute the Stokes parameters as follows:

$$
\begin{aligned}
I &= 1/2(I_0 + I_{22.5} + I_{45} + I_{67.5}),\\
Q &= I_0 - I_{45},\\
U &= I_{22.5} - I_{67.5},
\end{aligned}
$$

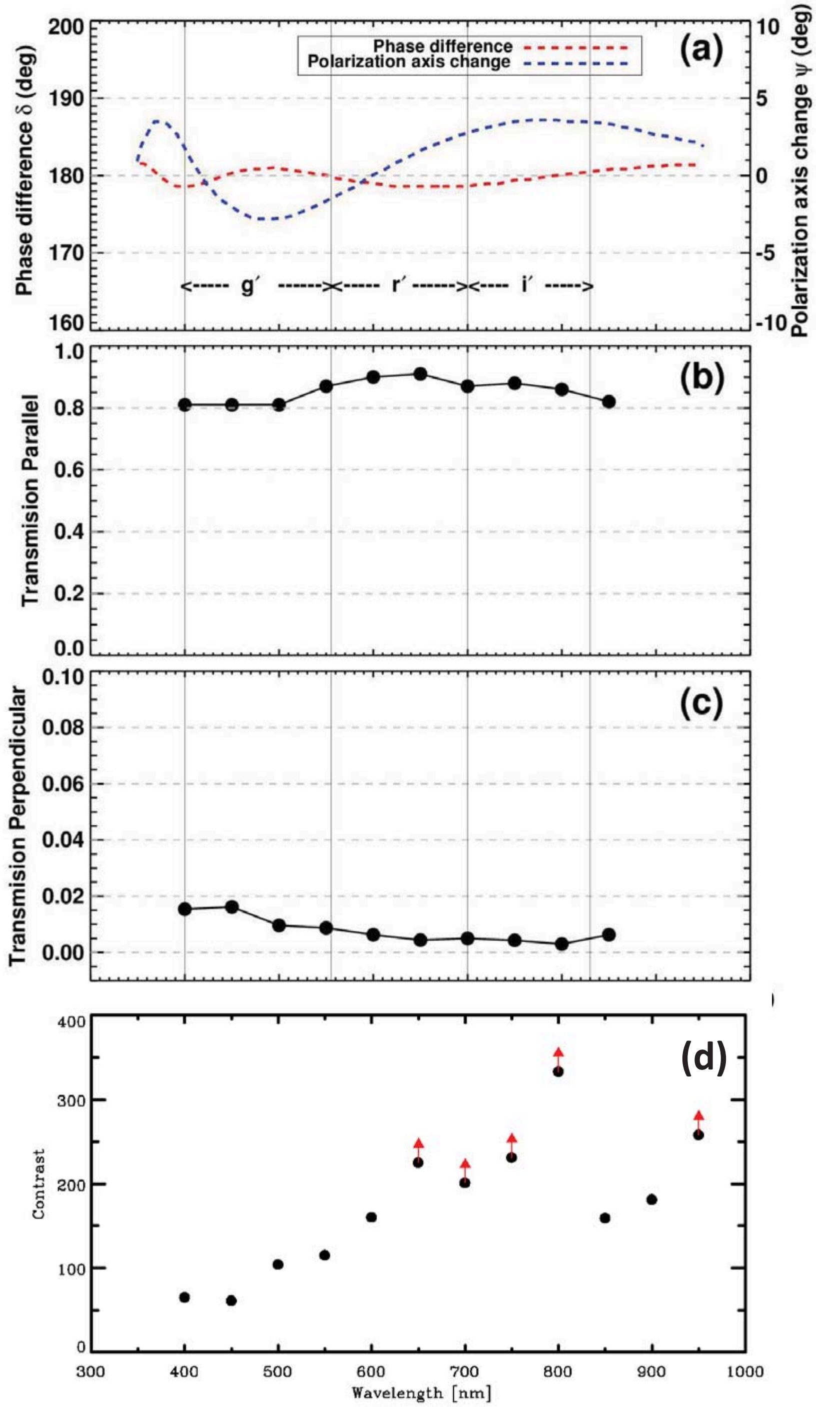

Fig. 3 Performance of the TRIPOL WGP: (a) the phase retardant (in units of deg); (b) transmittance with two polarizers in a parallel configuration; (c) transmittance with two polarizers in a perpendicular configuration; (d) contrast parameter ($T_{\max}/T_{\min}$). Those with a value greater than 200, each marked with an *upward arrow*, are uncertain because of a small number in the denominator.

where I_0, $I_{22.5}$, I_{45} and $I_{67.5}$ are the intensities at the four HWP angles in deg respectively, with the corresponding error being the square-root of the sum of the square of each intensity error, i.e., $\delta I = \sqrt{(\delta I_0)^2 + (\delta I_{22.5})^2 + (\delta I_{45})^2 + (\delta I_{67.5})^2}$. The errors δQ and δU are computed similarly.

The level of polarization P (in percentage) and the polarization position angle θ (in deg) are then derived accordingly,

$$P = \sqrt{Q^2 + U^2}/I,$$
$$\theta = 0.5 \arctan(U/Q),$$

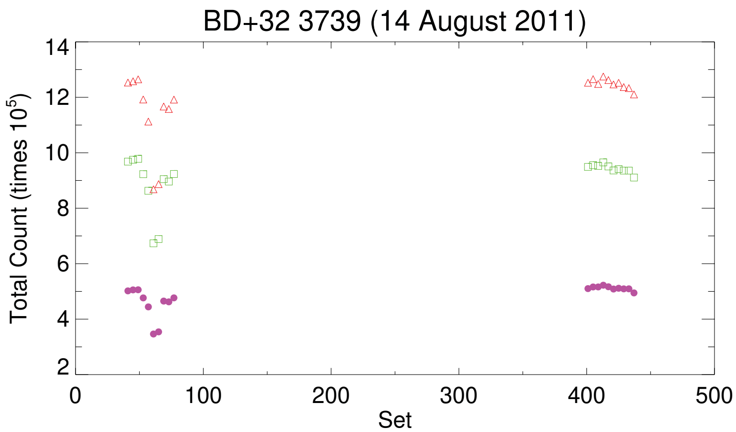

Fig. 4 The total counts of BD+32° 3739 showed inferior sky conditions in all g'- (in *green*), r'- (in *red*) and i'-bands for the first half of the night, whereas the sky was relatively stable in the second half.

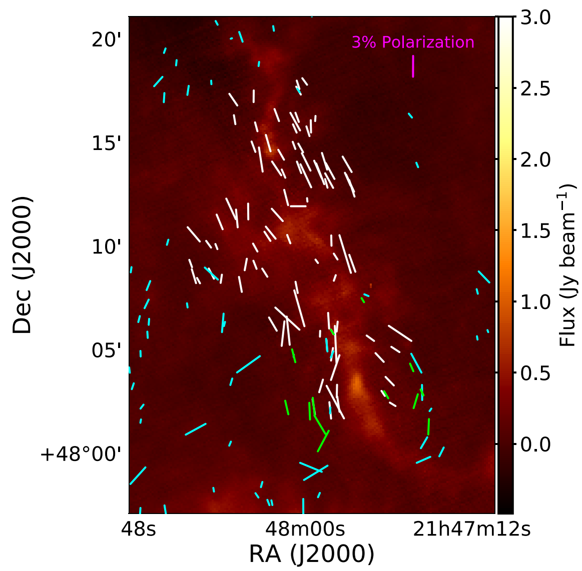

Fig. 5 TRIPOL i'-band polarization vector map (in *red*) of IC 5146 (Wang et al. 2017). The background image is the *Herschel* 250 μm data (Arzoumanian et al. 2011). Also shown are the polarization vectors measured by AIMPOL at R band (in *green*) and Mimir at near-infrared H band (in *blue*).

for which δP and $\delta\theta$ are estimated from the respective δQ and δU.

Because P is positively defined, the derived polarization is overestimated, especially for low S/N sources. To correct for this bias, the debiased value $P_{\rm db} = \sqrt{P^2 - (\delta P)^2}$ (Wardle & Kronberg 1974) is computed.

A polarization measurement relies on photometry at different polarization angles, and therefore all conditions pertaining to reliable photometric measurements apply. Even under a perfect photometric sky, though, our observations, via a fixed sequence of images taken at 0–45–22.5–67.5 deg, are subject to a small but noticeable flux drift due to airmass changes, leading to spurious polarization signals. Figure 4 depicts the results observed by LOT/TRIPOL on 2011 August 14 for BD+32° 3739, a standard star known to have null polarization (Schmidt et al. 1992). The total g' count, that is, the sum of $g'_0 + g'_{22.5} + g'_{45} + g'_{67.5}$, indicates varying sky conditions during the first session (a total of 10 sets of data, with each set consisting of images at four polarization angles per filter), starting at UT 12:53 (local time 20:53), but relatively stable skies during the second session (also with 10 sets), starting at local time 02:12. The ratio of the standard deviation of the total counts to the average counts, used as a measure of the sky stability, changed from about 13% in each of the g'-, r'- and i'-bands in the first session, to about 1% in the second session. The data taken in the first session hence should be discarded.

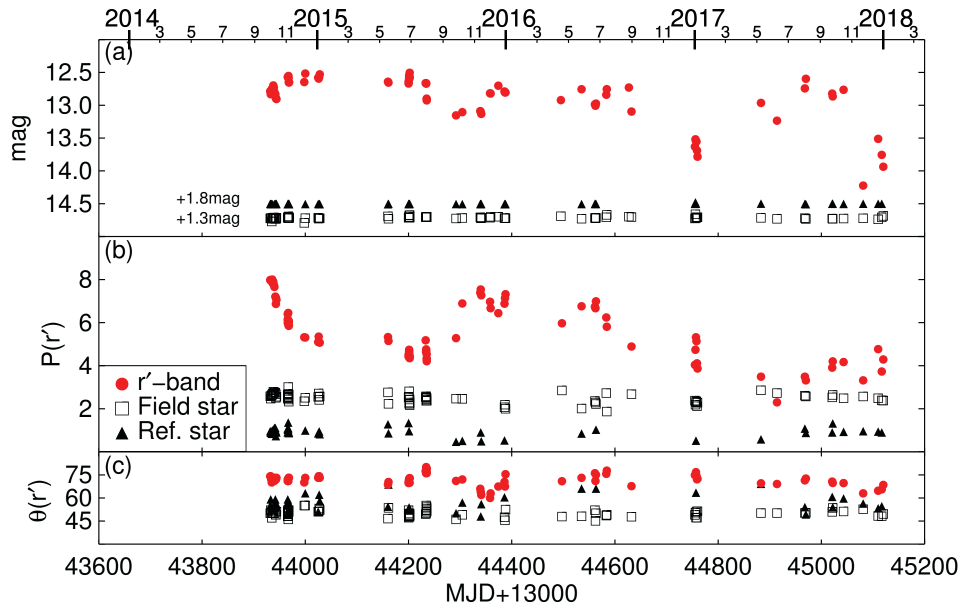

Fig. 6 The r'-band (a) light curve, (b) polarization and (c) polarization angle of the UX Ori-type young star GM Cep measured by TRIPOL from late 2014 to late 2017 (Huang et al. 2019). GM Cep shows a significant temporal change of polarization in comparison with two nearby stars.

Table 1 TRIPOL Measurements of Unpolarized Standard Stars

Star, mag/P_λ (Schmidt et al. 1992)	Date	$P_{g'}$ (%)	$P_{r'}$ (%)	$P_{i'}$ (%)
BD+32°3739, $V = 9.31$	2011 Aug 14	0.12 ± 0.11	0.12 ± 0.10	0.17 ± 0.15
$P_B = 0.039 \pm 0.021$	2011 Aug 15	0.14 ± 0.16	0.32 ± 0.14	0.19 ± 0.23
$P_V = 0.025 \pm 0.017$	2018 Oct 25	0.27 ± 0.27	0.26 ± 0.19	0.32 ± 0.18
	2018 Oct 28	0.20 ± 0.20	0.16 ± 0.16	0.17 ± 0.12
BD+28°4211, $V = 10.53$	2011 Aug 15	0.20 ± 0.19	0.34 ± 0.21	0.25 ± 0.10
$P_B = 0.063 \pm 0.023$	2011 Aug 17	0.08 ± 0.13	0.29 ± 0.14	0.32 ± 0.28
$P_V = 0.054 \pm 0.027$	2018 Oct 26	0.25 ± 0.12	0.20 ± 0.20	0.20 ± 0.20
$P_V = 0.054 \pm 0.027$	2018 Oct 27	0.28 ± 0.13	0.17 ± 0.17	0.21 ± 0.19
HD 212311, $V = 8.10$	2018 Oct 23	0.15 ± 0.05	0.15 ± 0.06	0.20 ± 0.05
$P_B = 0.028 \pm 0.025$	2018 Oct 24	0.20 ± 0.09	0.24 ± 0.06	0.13 ± 0.07
$P_V = 0.034 \pm 0.021$	2018 Oct 25	0.26 ± 0.12	0.23 ± 0.12	0.28 ± 0.14
	2018 Oct 26	0.11 ± 0.11	0.10 ± 0.15	0.32 ± 0.21
	2018 Oct 27	0.12 ± 0.12	0.23 ± 0.15	0.16 ± 0.16
	2018 Oct 28	0.07 ± 0.11	0.21 ± 0.10	0.12 ± 0.12

A further correction is the polarization introduced by the instrument, which is estimated by observing unpolarized standard stars. The mean and standard deviation of the measured polarization of unpolarized standards were found to be $P_{g'} = 0.27\% \pm 0.12\%$, $P_{r'} = 0.32\% \pm 0.23\%$ and $P_{i'} = 0.25\% \pm 0.13\%$. These values, summarized in Table 1, are considered as the instrumental polarization. For the unpolarized standard stars, with brightness up to $V \sim 12$ mag, the overall accuracy of polarization measurements with TRIPOL is estimated to be $\sim 0.3\%$ with an uncertainty of 3° for the polarization angle.

In every TRIPOL run, polarized standard stars should be observed to calibrate the measured polarization angle to the equatorial coordinate system. The TRIPOL measurements of a selected set of unpolarized standard stars and polarized stars are listed in Table 1 and Table 2 respectively, demonstrating general agreement with the published values, given that the observing wavelengths are slightly different. An observing run was carried out exclusively for

Table 2 TRIPOL Measurements of Polarized Standard Stars

Star/mag/P_λ, θ_λ (Schmidt et al. 1992)	Date	$P_{g'}(\%), \theta_{g'}$ (deg)	$P_{r'}(\%), \theta_{r'}$ (deg)	$P_{i'}(\%), \theta_{i'}$ (deg)
HD 154445, $V = 5.61$	2015 Feb 17	$3.8 \pm 0.1, 87 \pm 3$	$3.4 \pm 0.2, 82 \pm 2$	$3.7 \pm 0.1, 67 \pm 3$
$P_V = 3.780 \pm 0.062$, $\theta_V = 88.79 \pm 0.47$	2015 Feb 26	$3.8 \pm 0.1, 92 \pm 3$	$3.7 \pm 0.2, 90 \pm 2$	$3.7 \pm 0.1, 92 \pm 3$
$P_{Rc} = 3.683 \pm 0.072$, $\theta_R = 88.91 \pm 0.56$	2015 Feb 27	$3.8 \pm 0.1, 88 \pm 3$	$4.0 \pm 0.2, 86 \pm 2$	$3.5 \pm 0.1, 87 \pm 3$
$P_{Ic} = 3.246 \pm 0.078$, $\theta_I = 89.91 \pm 0.69$				
HD 161056, $V = 6.32$	2015 Feb 27	$3.9 \pm 0.1, 67 \pm 3$	$4.1 \pm 0.2, 66 \pm 2$	$3.7 \pm 0.1, 67 \pm 3$
$P_V = 4.030 \pm 0.025$, $\theta_V = 66.93 \pm 0.18$				
$P_{Rc} = 4.012 \pm 0.032$, $\theta_R = 67.33 \pm 0.23$				
$P_{Ic} = 3.575 \pm 0.030$, $\theta_I = 67.78 \pm 0.24$				
HD 204827, $V = 7.93$	2011 Aug 11	$5.5 \pm 0.2, 60 \pm 1$	$5.3 \pm 0.2, 61 \pm 1$	$4.7 \pm 0.2, 63 \pm 2$
$P_V = 5.322 \pm 0.014$, $\theta_V = 58.73 \pm 0.08$	2018 Oct 23	$5.5 \pm 0.3, 59 \pm 3$	$5.0 \pm 0.2, 58 \pm 2$	$4.5 \pm 0.3, 58 \pm 2$
$P_{Rc} = 4.893 \pm 0.029$, $\theta_R = 59.10 \pm 0.17$	2018 Oct 24	$5.8 \pm 0.2, 61 \pm 1$	$5.3 \pm 0.2, 60 \pm 1$	$4.5 \pm 0.2, 62 \pm 1$
$P_{Ic} = 4.189 \pm 0.030$, $\theta_I = 59.94 \pm 0.20$	2018 Oct 25	$5.9 \pm 0.1, 59 \pm 1$	$5.3 \pm 0.1, 60 \pm 1$	$4.5 \pm 0.1, 60 \pm 1$
	2018 Oct 26	$5.9 \pm 0.1, 57 \pm 1$	$5.2 \pm 0.0, 59 \pm 1$	$4.2 \pm 0.1, 60 \pm 1$
	2018 Oct 27	$5.6 \pm 0.2, 57 \pm 1$	$5.3 \pm 0.2, 58 \pm 1$	$4.4 \pm 0.2, 58 \pm 1$
	2018 Oct 28	$5.6 \pm 0.1, 59 \pm 1$	$5.1 \pm 0.1, 59 \pm 1$	$4.3 \pm 0.1, 60 \pm 1$
HD 19820, $V = 7.11$	2018 Oct 23	$4.5 \pm 0.1, 115 \pm 1$	$4.4 \pm 0.1, 115 \pm 1$	$4.2 \pm 0.1, 114 \pm 1$
$P_V = 5.322 \pm 0.014$, $\theta_V = 114.93 \pm 0.08$	2018 Oct 24	$4.6 \pm 0.2, 114 \pm 2$	$4.7 \pm 0.1, 111 \pm 1$	$4.0 \pm 0.1, 115 \pm 2$
$P_{Rc} = 4.893 \pm 0.029$, $\theta_R = 114.46 \pm 0.17$	2018 Oct 25	$4.9 \pm 0.2, 110 \pm 2$	$4.0 \pm 0.2, 115 \pm 2$	$4.5 \pm 0.1, 117 \pm 2$
$P_{Ic} = 4.189 \pm 0.030$, $\theta_I = 114.48 \pm 0.20$	2018 Oct 26	$4.2 \pm 0.1, 111 \pm 2$	$3.8 \pm 0.1, 113 \pm 1$	$3.5 \pm 0.1, 115 \pm 2$
(Variable, this work)	2018 Oct 27	$4.4 \pm 0.1, 111 \pm 1$	$4.3 \pm 0.1, 113 \pm 1$	$3.6 \pm 0.1, 115 \pm 1$
	2018 Oct 28	$4.6 \pm 0.2, 114 \pm 1$	$4.6 \pm 0.2, 113 \pm 1$	$4.0 \pm 0.1, 113 \pm 1$

standard star calibration in October 2018 to assess the intranight and internight consistency of the TRIPOL measurements. For unpolarized standard stars, accuracy is kept to two decimal digits, and no polarization angle is listed. For polarized standard stars, the fractional polarization is kept to one decimal digit, with the polarization angle in integers reflecting the uncertainties. In the October 2018 run, each target was measured a few times, and the entries in Table 1 and Table 2 for each date are the average values of individual measurements and the associated errors. Because we relied on the standard stars to correct for the polarization angles (one offset per night for each angle at each band), the values of angles scatter around the offset. From the observations of polarization standards, we conclude that the WGP has a high efficiency for measuring polarized light, and there is no need to correct for instrumental polarization, except for an angular offset.

Note that only standard stars from Schmidt et al. (1992) known not to vary were selected. In the process of our experiment, we found that one target, HD 19820, however, exhibited noticeable variability in the polarization level, but with a relatively steady polarization angle in our measurements. The mechanism of variability is unclear, but this O-type star is reported to be a binary system with a period of 3.366324 d (Hilditch & Hill 1975; Hill et al. 1994). Its polarization variability requires further study but, in any case, using it as a standard is not advisable.

4 SCIENTIFIC DEMONSTRATION

Data acquired by TRIPOL provide simultaneous information such as flux, linear polarization and the source coordinates in three bands, enabling study of the spectral energy distribution (SED), color-magnitude and color-color diagrams, and polarization. The combination of wavelength-dependence on polarization with the SED could distinguish various emission and propagation processes, such as synchrotron emission, scattering or extinction.

For imaging photometry, the time resolution of TRIPOL is as fast as about 1 s, whereas for polarimetry it is $\sim$ 15 s. As a single-beam instrument, TRIPOL is susceptible to polarization caused by the instrument itself, and to sky variations. The effects of internal polarization are assessed by observing standard stars. To mitigate the sky effects, multiple sets of observations are taken, and those with comparable total counts in four polarization angles are used in polarization analysis. This compromises the time resolution to a few minutes, but because of the simultaneity in three bands, TRIPOL still proves efficient. TRIPOL should be especially useful for investigating variable phenomena on timescales from a few seconds to years or longer. These include, but are not limited to, gravitational wave counterparts (Morokuma et al. 2016), gamma-ray bursts, cataclysmic variables, eclipsing binaries, Cepheids, novae, supernovae, blazars, Miras and T Tauri stars (Chen et al. 2015; Huang et al. 2019).

We are pursuing several programs for polarimetric monitoring of Galactic star-forming regions. An organized polarization pattern of background stars, as a result of dichroic extinction by magnetically aligned dust grains, provides the magnetic field structure in a dark cloud (Davis & Greenstein 1951), whereas scattered light reveals the radiation fields and spatial distribution of circumstellar matter of young stellar objects. Polarimetric observations with TRIPOL2 on the LOT were carried out for IC 5146 on 2012 July 27 and 28. Seven fields were observed toward the northwest part of this filamentary cloud, with a total exposure time of 1.5 h (22.5 min for each HWP angle). Polarization measurements simultaneously acquired in g'-, r'- and i'-bands were corrected for both instrumental polarization as well as offset polarization angles by observing polarized and unpolarized standard stars. Figure 5 displays the i'-band polarization of the northwest part of IC 5146 (Wang et al. 2017).

Also plotted in Figure 5 are the ARIES Imaging Polarimeter (AIMPOL) R-band and Mimir H-band polarization data. AIMPOL (Reutela et al. 2004), an optical polarimeter installed on the 1.04 m Sampurnanand Telescope of ARIES in Nainital, India, has been calibrated well over the years by observing unpolarized and polarized standard stars (Medhi et al. 2007; Eswaraiah et al. 2013). Mimir is a near infrared imager for polarization measurements (Clemens et al. 2007) mounted on the 1.8 m Perkins Telescope in Arizona, operated by Lowell Observatory.

While TRIPOL2 and Mimir observations each covered a larger part of the filament than AIMPOL data did, the polarization results measured by the three instruments, two working in optical and one in near infrared, are consistent with each other, suggesting a global magnetic field roughly parallel to the long axis of the filament. On average, TRIPOL2 detected more prominent polarization than Mimir, a manifestation of higher fractional polarization in visible wavelengths because the extinction difference is amplified. Infrared polarimetry, on the other hand, probes denser parts of a molecular cloud. A combination of optical and infrared polarimetry, together with millimeter and submillimeter interferometric observations of polarization, hence offers an opportunity to scrutinize the magnetic field structure at scales from a cloud core to the central protostar. Detailed results on IC 5146 can be found in Wang et al. (2017).

Another application of TRIPOL is targeting the point source GM Cep, a 4-Myr T Tauri star undergoing abrupt photometric variations caused by obscuration of protoplanetary dust clumps (Chen et al. 2012; Chen & Hu 2014; Huang et al. 2019). The long-term photometric and polarimetric monitoring data, plotted in Figure 6, display a noticeable polarization up to 8% with temporal variability on a timescale of years, while the comparison star exhibits a steady level of polarization, with a standard deviation of less than 1%. Such polarization observations provide valuable information on the distribution and properties of the circumstellar dust clumps, from grain growth from micron-size dust in transition to km-size planetesimals (Huang et al. 2019).

5 SUMMARY

The simultaneous three-color (g', r', i') polarimeter, TRIPOL, is simple, compact and economical, suitable for a small telescope at a moderate astronomical site. This paper presents the design concept and compares the performance to data taken on the LOT located in Taiwan. The limiting magnitudes for photometry are found to be $g' \sim 19$ mag, $r' \sim 18.5$ mag and $i' \sim 18$ mag, with an S/N of 10 and an integration time of 100 s. The internal instrumental polarization is at the level of 0.3% for a 100-s integration at all three bands. The simultaneous photometric and polarimetric capability should open up new research opportunities for time-domain astronomy on small or amateur telescopes.

Acknowledgements We are grateful to N. Takeuchi and A. Yamanaka for their laboratory experiments, and to Drs. M. Kino, M. Kurita, T. Nagayama, K. Kawabata, M. Ishiguro and H. Takami for valuable comments throughout the development of this project. We appreciate Dr. Y. Nakajima for his kind assistance with the data reduction and Drs. M. Ishiguro and K Murata for preparation of the figures. This work is supported by Grant-in-Aid for Science Research from the Ministry of Education, Culture, Sports and Technology of Japan. SS owes his scientific activity to Dr. H. Fujiwara for his generous support of astronomy.

References

Arzoumanian, D., André, P., Didelon, P., et al. 2011, A&A, 529, L6

Chen, W. P., Hu, S. C.-L., Errmann, R., et al. 2012, ApJ, 751, 118

Chen, W. P., & Hu, S. C.-L. 2014, in IAU Symposium, 293, Formation, Detection, and Characterization of Extrasolar Habitable Planets, ed. N. Haghighipour, 74

Chen, W. P., Su, B. H., Eswaraiah, C., et al. 2015, Highlights of Astronomy, 16, 390

Clarke, D. 2010, Stellar Polarimetry (Wiley)
Clemens, D. P., Sarcia, D., Grabau, A., et al. 2007, PASP, 119, 1385
Davis, Jr., L., & Greenstein, J. L. 1951, ApJ, 114, 206
Hilditch, R. W., & Hill, G. 1975, MmRAS, 79, 101
Hill, G., Hilditch, R. W., Aikman, G. C. L., & Khalesseh, B. 1994, A&A, 282, 455
Huang, P. C., Chen, W. P., Mugrauer, M., et al. 2019, ApJ, 871, 183
Kandori, R., Kusakabe, N., Tamura, M., et al. 2006, in Proc. SPIE, 6269, 626951
Landolt, A. U. 1992, AJ, 104, 340
Morokuma, T., Tanaka, M., Asakura, Y., et al. 2016, PASJ, 68, L9
Rautela, B. S., Joshi, G. C., & Pandy, J. C. 2004, BASI, 32, 159
Schmidt, G. D., Elston, R., & Lupie, O. L. 1992, AJ, 104, 1563
Tinbergen, J. 1996, Astronomical Polarimetry (Cambridge, UK: Cambridge Univ. Press), 174
Wang, J.-W., Lai, S.-P., Eswaraiah, C., et al. 2017, ApJ, 849, 157
Wardle, J. F. C., & Kronberg, P. P. 1974, ApJ, 194, 249